

**MOLECULAR DYNAMICS SIMULATION OF
THERMAL PROCESSES FOR SELECTED NANO-
STRUCTURES**

by

MIN TJUN KIT

Thesis submitted in fulfillment of the requirements

for the degree of

Master of Science

September 2018

ACKNOWLEDGEMENT

First of all, I wish to express my gratitude to my supervisor, Dr. Yoon Tiem Leong, for their professional guidance and suggestions throughout the whole period of my project and thesis writing. The same also goes to Dr. Lim Thong Leng from Multimedia University, Melaka, who has provided a lot of inspiring guidance and academic advice to make the work in this thesis a success. I would like to acknowledge the collaboration with the Complex Liquid Lab, National Central University, Taiwan, led by Prof. Lai San Kiong, along with his group members, for their academic support. Ideas, motivation, comments as well as the tireless commitment from individuals mentioned above are essential contributing factors in leading my learning path to become a researcher. For their help and concerns in my studies, I am greatly indebted to all of them.

I would like to thank the Ministry of Higher Education for financial support in term of Fundamental Research Grant Scheme (FRGS) (Project number: 203/PFIZIK/6711348) as well as MyMaster scholarship in covering the tuition fees.

For the immediate colleagues from the theoretical and computational group, I would like to thank them for helping me in my research and pleasantly accommodate my presence. We shared many fruitful discussions that involved a lot of general knowledge, essentially a wide coverage on the latest world news that brings insights to each of us. Special thanks to Mr. Ng Wei Chun, my junior who has offered all kinds of support. Next in line are juniors Ms. Soon Yee Yeen and Ms. Ong Yee Pin for their help in organizing various meetings and sharing of paperwork.

Last but not least, I am grateful for my family who supports me in all aspects. They understand and respect my decisions during the completion of my project, and thesis. The hard works and sacrifices they have made encourage me even more to succeed both in life and in academic.

TABLE OF CONTENTS

Acknowledgement	ii
Table of Contents	iv
List of Tables	vii
List of Figures	viii
List of Abbreviations	xiii
Abstrak	xiv
Abstract	xvii
CHAPTER 1 - INTRODUCTION	1
1.1 Motivation of Study	1
1.2 Problem statements	3
1.3 Objectives	4
1.4 Overview of the thesis	5
CHAPTER 2 - BACKGROUND THEORY	6
2.1 Carbon Nanostructures	6
2.2 Epitaxial Growth of Graphene	11
2.3 Silicene	13
2.4 Zinc Oxide	15

2.5	Molecular Dynamic Simulation	17
CHAPTER 3 - RESEARCH METHODOLOGY		20
3.1	Epitaxial Growth of Graphene	20
3.1.1	Empirical Potential	20
3.1.2	Construction of 6H-SiC substrate	22
3.1.3	Simulation Details	31
3.2	Melting of Silicene	32
3.2.1	Empirical Potential	32
3.2.2	Construction of silicene	33
3.2.3	Simulation Details	34
3.2.4	Global Similarity Index	36
3.3	Annealing of ZnO surfaces	39
3.3.1	Structure of ZnO	39
3.3.2	Simulation Details	40
3.3.3	Empirical Potential	42
CHAPTER 4 - RESULTS AND DISCUSSION		44
4.1	Epitaxial Growth of Graphene	44
4.1.1	Binding Energy of Graphene	44
4.1.2	One-layer Graphene	45

4.1.3	Double-layered Graphene	53
4.1.4	Three-layer Graphene	59
4.2	Melting of Silicene	61
4.3	Annealing of ZnO surfaces	69
4.3.1	Sublimation of O atoms at and beyond a threshold temperature T_t	69
4.3.2	Ratio of surface O atoms sublimated as a function of annealing temperature	69
4.3.3	Sublimation of surface O atoms in pairs	70
4.3.4	Comparison with results from experiment measurements	71
4.3.5	Partial charge distribution	74
4.3.6	Partial charge of the sublimated O atoms	81
4.3.7	The Zn-terminated surfaces, (0 0 0 1)	82
CHAPTER 5 - CONCLUSIONS AND RECOMMENDATIONS		83
REFERENCES		85
LIST OF PUBLICATIONS		

LIST OF TABLES

	Page
Table 3.1 LAMMPS input requires for the data files which provides information required for constructing a rhombus shape 6H-SiC substrate. The information is extracted from http://cst-www.nrl.navy.mil/lattice/struk/6h.html .	23
Table 3.2 Crystal structure of wurtzite ZnO, as obtained from [54].	39

LIST OF FIGURES

	Page
Figure 2.1	Types of carbon nanotubes and its chirality. 7
Figure 2.2	Low-dimensional carbon allotropes: fullerene (0-D), carbon nanotube (1-D) and graphene (2-D). 7
Figure 2.3	The nanotubes and its chiral angle. 9
Figure 2.4	Single wall nanotube (left) and multiwall nanotube (right). 10
Figure 2.5	A graphite structure. 10
Figure 2.6	(a) The structure of a free-standing silicene, (b) the bond length and bond angle of silicene and (c) the buckling parameter of a silicene. 14
Figure 2.7	Periodic boundary condition of molecular dynamics. Each particle not only interacts with every other particle in the system but also with all other particles in the copies of the system. The arrows from the particles point to nearest copy of other particles in the system [46]. 19
Figure 3.1	Visualization of the SiC unit cell. Si atom is in light blue. The type of atom can be read off from column 3 in the inset. The z-coordinate of each atom, which are labeled No. 1 to No. 12 in the first column of the inset, are clearly shown in the last column of the inset. 25
Figure 3.2	The unit cell as shown in Fig. 3.1, when repeated along the x-direction and y-direction via periodic boundary condition will form an infinite substrate along these two directions as shown, in which the structure is viewed from the sideway (i.e., from the x-direction). 26
Figure 3.3	Substrate of Si-terminated 6H-SiC (0001) taken as the initial configuration input in LAMMPS software for performing simulated annealing. Standard periodic conditions are applied along the x- and y-directions. 27
Figure 3.4	Figure 3.4: Modified 6H-SiC substrate after removing the Si atom (that labelled No. 2 in Fig. 3.1) and replacing it by the 28

C atom (that labelled No. 1 in Fig. 3.1).

- Figure 3.5 Preparation of a two C-rich bilayers substrate for growing a two-layer graphene. This is done by systematically relocating the atoms in the original unit cell of Fig. 3.1. The essential separations between the atom layers are labelled. The system is then energy-minimized. The values in black and red are those before and after energy minimization. The value $L = 1.35 \text{ \AA}$ is found by manual tuning (see text). 30
- Figure 3.6 A silicene sheet created from diamond structure of silicon in Si (1 1 1) orientation. It is a 2D honeycomb shape similar to graphene (left) with dimensions of $130.563 \text{ \AA} \times 150.761 \text{ \AA}$ and buckling parameter of 0.44 \AA (right). The average bond length of Si-Si is 2.4 \AA . 34
- Figure 3.7 The $15 \times 15 \times 1$ supercell of wurtzite ZnO slab used as initial structure in this MD simulation. Left: Direct surface view from the direction $+z$; Right: Edge-on view. The $(0\ 0\ 0\ \bar{1})$ surface terminates with oxygen atoms while $(0\ 0\ 0\ 1)$ Zn atoms. In these figures, the $(0\ 0\ 0\ \bar{1})$ surface is in the direction pointing along $+z$, while the $(0\ 0\ 0\ 1)$ surface in the $-z$ direction 40
- Figure 3.8 A typical temperature vs. step profile in the simulation. 41
- Figure 4.1 The binding energy (per atom) E_b for an infinite free graphene layer calculated with the Tersoff (solid circles or dashed line) and TEA (open circles or full line) potentials at different values of lattice constant a_0 . 45
- Figure 4.2 One-layer graphene overlaid on Si-terminated 6H-SiC (0001) obtained by the simulated annealing method for (a) Tersoff (second column) and (b) TEA (third column) potentials. In the second and third columns at the bottom corner on the right, the integer is the hexagon number. The average distance of separation between the graphene buffer layer and surface is about 2.43 \AA for TEA potential. 46
- Figure 4.3 The variation of the binding energy (per atom) E_b plotted against the equilibrium annealing time steps ($\Delta t = 0.5 \text{ fs}$) at (a) 1200 K for Tersoff potential, (b) 1100, and (c) 1200 K for TEA potential. 48
- Figure 4.4 Comparison of the average bond-length l (\AA) versus annealing temperature T (in units Kelvin) between results 50

calculated using TEA (open circle) and Tersoff (solid circle) potentials.

- Figure 4.5 Same as Fig. 4.4 except for the binding energy (per atom) E_b . 50
- Figure 4.6 (a) Pair correlation function $g(r)$ of carbon atoms obtained using TEA potential at different annealing temperature T (in units of Kelvin) for the one-layer graphene which emerges for $T \geq 1200$ K. At $T < 1200$ K, it displays typical crystalline structure. (b) Same as Fig. 8(a) except that the MD simulations were done using Tersoff potential. The one-layer graphene emerges at $T \geq 1500$ K. At $T < 1300$ K, it displays typical crystalline structure. Only few hexagons are seen at $T = 1400$ K. 52
- Figure 4.7 The result of binding energy against temperature when the substrate used is with thickness 15.11 \AA (or $Z = 1$), it is hard to pinpoint the formation temperature of graphene when the substrate is too thin. The overall structure has very poor thermal stability. 54
- Figure 4.8 A 6H-SiC unit cell with a thickness $Z = 2$ substrate. 55
- Figure 4.9 Two-layer graphene overlaid on 6H-SiC (0001) obtained by simulated annealing method with TEA potential. In the second and third columns at the bottom corner on the right, the integer is the hexagon number. 57
- Figure 4.10 (a) The average bond-length (\AA) versus annealing temperature T (in units of Kelvin) obtained by the simulated annealing using TEA potential for two-layer graphene. Notations used are: first-layer graphene, open circle; second-layer, solid circle. (b) The binding energy (per atom) E_b (in units of eV) versus annealing temperature T (in units of Kelvin) obtained by simulated annealing using TEA potential for two-layer graphene. 58
- Figure 4.11 Three-layer graphene overlaid on 6H-SiC (0001) obtained by simulated annealing method with TEA potential. The first graphene “buffer” layer refers to one closest to the top surface of substrate and has an average distance of separation about 2.6 \AA , and the third layer corresponds to one next to the second graphene layer and these graphene layers are separated by an average distance about 3.2 \AA . And the separation between the second layer and the first layer 59

(the top most layer) is 2.8 Å.

- Figure 4.12 (a) The binding energy (per atom) E_b (in units of eV) versus annealing temperature T (in units of Kelvin) obtained by simulated annealing using TEA potential for three-layer graphene. (b) The average bond-length (Å) versus annealing temperature T (in units of Kelvin) obtained by the simulated annealing using TEA potential for three-layer graphene. The result above shown is only applied for the third-layer graphene. 60
- Figure 4.13 Simulated annealing of silicene by using optimized Stillinger-Weber potential. Initially the silicene has equilibrium bond length of ~ 2.5 Å. An abrupt change can be viewed at 1500 K in which the sheet is tearing apart and the melting process is thus begins. After the melting point, the Si particles settle down to form four smaller “islands” which has equilibrium bond length of ~ 2.8 Å. 65
- Figure 4.14 (Continuation from Figure 4.13) 66
- Figure 4.15 Pair correlation function of the system at various temperatures. At room temperature a sharp peak occurs at ~ 2.5 Å. The distribution curve begins to widen up and the peak at ~ 2.5 Å is lowered as target temperature T increases. 67
- Figure 4.16 Potential energy plot (caloric curve) of the system (eV) against temperature (K) measured for target temperature, $T = 2000$ K. The sharp and abrupt drop of potential energy at 1500 K indicates occurrence of melting at that temperature. 67
- Figure 4.17 Global similarity index plot against temperature. The silicene structure is compared with its 300 K state. 68
- Figure 4.18 Amorphous silicon “cylinder” after quenching of the melted silicene. The structure is unable to revert to a sheet form. 68
- Figure 4.19 Ratio of O atoms sublimated (normalized to original number of O atoms on the surface) for $T = 300$ to 1300 K 70
- Figure 4.20 Snapshots at various stages of the partial charge distribution in the ZnO slab when undergoing annealing at $T = 300$ K. (a) At the beginning, the slab of ZnO has only gone through energy minimization at 0.1 K but not any thermal treatment. (b) and (c) are snapshots during which the slab is being 77

annealed at the temperature plateau T . (d) Slab at the end of thermal history as depicted by Fig. 3.8. The vertical axis is in units of e . The z -axis is in units of \AA

- Figure 4.21 Snapshots at various stages of the partial charge distribution in the ZnO slab when undergoing annealing at $T = 1300$ K. 78
- Figure 4.22 Partial charge distributions at the end of an MD run for eight annealing temperatures ranging from 400 K to 1100 K. 79
- Figure 4.23 Charge density $\rho(z)$ as a function of depth from the $(0\ 0\ 0\ \bar{1})$ surface, z , for annealing temperature $T = 500$ K, $T = 700$ K, $T = 800$ K and $T = 1000$ K. The vertical axis is in units of $e/\text{\AA}^3$. The z -axis is in units of \AA . Note the qualitative change of the density profile (especially the region close to the $(0\ 0\ 0\ \bar{1})$ end) when crossing from $T = 700$ K to $T = 800$ K 80
- Figure 4.24 Average partial charge per sublimated atom as a function of annealing temperature. 81

LIST OF ABBREVIATIONS

CNT	Carbon Nanotube(s)
MD	Molecular Dynamics
LAMMPS	Large-scale Atomic/Molecular Massively Parallel Simulator
TEA	Tersoff-Erhart-Albe
SW	Stillinger-Weber
NVT	Nose-Hoover thermostat, constant number (N), volume (V), and temperature (T)
NVE	Canonical Ensemble, constant number (N), volume (V), and energy (E)
ReaxFF	Reactive Force Field
EEM	Electronegativity Equalization Method
COMB	Charged Optimized Many Body
PL	Photoluminescence

SIMULASI DINAMIK MOLEKUL UNTUK PROSES TERMA BAGI STRUKTUR NANO YANG TERPILIH

ABSTRAK

Premis utama dalam tesis ini adalah menggunakan kaedah dinamik molekul (MD) untuk menyimulasi dan mengukur tiga sistem nano yang berbeza, termasuklah (i) pertumbuhan grafen secara epitaksial pada permukaan 6H-SiC (0001) yang didorongkan oleh pemanasan simulasi, (ii) *silicene* yang tergantung bebas tertakluk kepada pemanasan yang ekstensif, dan (iii) kepingan ZnO berbentuk wurtzite yang tertakluk kepada pemanasan simulasi. Pertumbuhan grafen secara epitaksial pada permukaan (0001) daripada substrat 6H-SiC disimulasikan melalui kaedah dinamik molekul dengan menggunakan kod LAMMPS. Pembentukan grafen secara epitaksial di permukaan substrat disimulasikan melalui satu protocol yang direka khas untuk mencapai pembinaan semula permukaan. Dua keupayaan empirik, iaitu keupayaan Tersoff dan keupayaan TEA digunakan dalam simulasi MD supaya mekanisme pertumbuhan yang dipaparkan oleh mereka dapat diselidiki dan dibandingkan. Keputusan yang diperolehi daripada simulasi MD dalam tesis ini menunjukkan bahawa keupayaan TEA lebih tepat dalam menggambarkan proses pertumbuhan untuk membentuk grafen, di mana keputusannya adalah lebih fizikal dan realistik secara umumnya. Dalam simulasi MD dengan menggunakan keupayaan TEA, grafen muncul secara tepat pada suhu pemanasan ~ 1200 K, setanding dengan yang diperhatikan dalam eksperimen yang dilaporkan di mana grafen ternukleat pada suhu pembentukan lubang 1298 K. Penilaian secara berangka ke atas panjang ikatan purata, tenaga ikatan serta fungsi korelasi pasangan dalam eksperimen MD membenarkan pengukuran dan kuantifikasi dilakukan ke atas grafen yang terbentuk.

Grafen yang berlapisan dua dan tiga boleh ditumbuh berdasarkan substrat yang sama selepas lapisan grafen pertama dibentuk. Teknik untuk menumbuh grafen berlapisan dua dan tiga di atas grafen lapisan tunggal yang sedia terbentuk menyerupai prosedur untuk menumbuh grafen lapisan pertama dengan sedikit pemubahsuaian. Selain daripada pertumbuhan grafen secara epitaksial, tesis ini juga melakukan simulasi MD untuk mengukur takat lebur *silicene* yang tergantung bebas dengan menggunakan keupayaan Stillinger-Weber (SW) yang dioptimumkan oleh Zhang et al.. Data ini dianalisis secara sistematik dengan menggunakan beberapa petunjuk yang berbeza secara kualitatif, termasuk fungsi lengkung kalori, fungsi taburan jejarian dan petunjuk berangka yang dikenali sebagai indeks kesamaan global. Keupayaan SW yang dioptimumkan menghasilkan takat lebur secara konsistennya pada 1500 K untuk simulasi *silicene* yang tergantung bebas serta tak-terhingga. Sistem berskala nano yang ketiga yang disiasat dalam tesis ini melalui MD adalah kepingan ZnO yang tebal berbentuk wurtzite yang ditamatkan pada dua permukaan, iaitu $(000\bar{1})$ (yang ditamatkan oleh oksigen) dan (0001) (yang ditamatkan oleh Zn). Eksperimen MD dilakukan untuk mengukur kesan pemanasan haba ke atas kepingan ZnO. Untuk tujuan ini, medan daya reaktif (ReaxFF) digunakan. Sebagai akibat pemanasan, untuk julat suhu ambang $700 \text{ K} < T_t \leq 800 \text{ K}$, permukaan oksigen mula memejalwap dari permukaan $(000\bar{1})$, sementara tiada atom meninggalkan permukaan (0001) . Nisbah oksigen yang meninggalkan permukaan meningkat dengan peningkatan suhu T (untuk $T \geq T_t$). Keamatan kependarkilauan relatif pada puncak sekunder dalam spektrum foto-kependarkilauan (PL), ditafsirkan sebagai ukuran jumlah kekosongan pada permukaan sampel, bersetuju dengan simulasi MD secara kualitatif. Simulasi MD juga mendedahkan pembentukan dimer oksigen di permukaan serta evolusi pengagihan caj separa

semasa proses pemanasan. Keputusan daripada simulasi MD berdasarkan ReaxFF adalah konsisten dengan pemerhatian eksperimen.

MOLECULAR DYNAMICS SIMULATION OF THERMAL PROCESSES FOR SELECTED NANO-STRUCTURES

ABSTRACT

The core premise of this thesis is the adoption of molecular dynamics (MD) in simulating and measuring three different nanoscale systems. namely (i) epitaxial graphene growth on 6H-SiC (0001) surface induced by simulated annealing, (ii) free-standing silicene subjected to extensive thermal heating, and (iii) wurtzite ZnO slab which is subjected to simulated annealing. Epitaxial growth of graphene on the (0001) surface of 6H-SiC substrate is simulated via molecular dynamics using LAMMPS code. A specially designed protocol to reconstruct the surface via a simulated annealing procedure, is prescribed to simulate the epitaxial graphene formation on the substrate surface. Two empirical potentials, the Tersoff potential and the TEA potential are used in the MD simulations to investigate and compare the growth mechanisms resulted. Results obtained from MD simulated in this thesis show that TEA potential is more accurately in describing the growth process of graphene formation, in which the result is generally more physical and realistic. Graphene is shown in the MD simulation using TEA potential to be accurate at an annealing temperature of $T \approx 1200$ K, comparable to that observed in a reported experiment in which graphene nucleates at a pit-forming temperature of 1298 K. The numerical evaluation of the average bond-length, binding energy as well as pair correlation function in the MD experiments allows for the measurement and quantification of the graphene formed. Double and triple layer graphene can also be grown from the same substrate after the first layer of graphene is formed. The technique to grow double and triple layer graphene on top of the already-formed single layer graphene follows

a similar but slightly modified procedure used in growing the first layer graphene. In addition to epitaxial graphene growth, MD simulations are also performed in this thesis to measure the melting temperature of free-standing silicene by using optimized Stillinger-Weber (SW) potential by Zhang et al.. The data are systematically analysed using a few qualitatively different indicators, including caloric curve, radial distribution function and a numerical indicator known as global similarity index. The optimized SW potential consistently yields a melting temperature of 1500 K for the simulated free-standing, infinite silicene. The third nanoscale system investigated in this thesis via MD is a thick wurtzite ZnO slab terminated in two surfaces, namely, $(000\bar{1})$ (which is oxygen terminated) and (0001) (which is Zn-terminated). The MD experiment is performed to measure the effect of thermal annealing on the ZnO slab. To this end, reactive force field (ReaxFF) is used. It is observed that annealing results in the sublimation of surface oxygen atoms from the $(000\bar{1})$ surface at a threshold temperature range of $700\text{ K} < T_t \leq 800\text{ K}$, while no atoms leave the (0001) surface. The ratio of oxygen leaving the surface increases with temperature T (for $T \geq T_t$). The relative luminescence intensity of the secondary peak in the photoluminescence (PL) spectra, interpreted as a measurement of amount of vacancies on the sample surfaces, qualitatively agrees with the threshold behaviour as found in the MD simulations. The formation of oxygen dimers on the surface and evolution of partial charge distribution during the annealing process has also been depicted in the MD simulations. The MD simulations have also revealed the formation of oxygen dimers on the surface and evolution of partial charge distribution during the annealing process. The results from the MD simulations based on the ReaxFF are consistent with experimental observations.

CHAPTER 1: INTRODUCTION

1.1 Motivation of Study

The discovery of graphene has opened a doorway to endless possibility in material science that no one can imagine. It sparks a field of debate and controversial (especially germanene and stanene which is still hypothetical [1] among material scientists. The experimental discovery of graphene in particular, and other 2D nanomaterials in general, have since driven researchers to intensify research effort to investigate their respective properties which has proven tremendous applications such as a substitution to our current conventional devices. Since the discovery of the graphene in 2010, it has revolutionized the field of material science. Many researchers around the world have since delved into the field of low dimensional structure in the hope to utilize graphene for wide range of application especially in nanoelectronics and N/MEMS. But now, they even look for the alternative for graphene (i.e. silicene, germanene, stanene and heterostructure of 2D materials) [1] to further improve the performance of various devices.

One of the interests in studying low dimensional nanostructures is their enhanced properties due to scaling effect as compared to their respective bulk properties. By understanding the properties of the nanostructures (i.e. thermodynamical properties, electronic properties, optical properties etc.) equips us with the necessary knowledge to turn them into applications. For example, a nanostructure with high thermal and electrical conductivity is suitable for fabrication of computer nanochip which is small, high in operating efficiency, saving electricity and generating less heat. In order to turn nanomaterials into real applications, it is

necessary to understand the technique to produce high quality nanostructures with minimum defect. Growing a large surface area of 2D nanostructures with minimum defect is a desirable achievement among material scientists working in the field.

However, experimental investigation on materials at nanoscale requires high precision technologies and can often be difficult to carry out in practice. Detailed dynamics occurring at atomistic level in these nanomaterials demands expensive and ultraprecision technique if it is to be revealed experimentally. However, there are alternative approaches to physically measuring these nanosystems for atomistic information, e.g., computational approach, of which molecular dynamics (MD) is an excellent representative. Nanomaterials, which are made up of atoms and molecules that interact among themselves via potential fields (a. k. a force fields) at classical level, can be simulated by building atomistic models that mimic their realistic behavior. Time evolution of the dynamical details in the simulated systems can be followed atom-by-atom. In this way, many physical properties, such as thermodynamical and mechanical properties, can be derived from ensembles of atoms mimicking these nanomaterials by applying classical physics and standard statistical mechanics techniques on the molecular dynamics data. Despite not able to capture physical properties of nanomaterials that are driven by quantum mechanical effect (generally known as the electronic structures), molecular dynamics is still a powerful, convenient and relatively cheap way to simulate nanomaterials at atomistic scale. The study of this thesis resolves around the theme of simulating thermal properties of low dimensional nanostructures of three distinct systems via molecular dynamics simulation.

1.2 Problem Statements

To reveal the temperature-driven dynamics of the atoms making up materials at nanoscale via experimentation techniques requires expensive and ultra-precision equipment. It is not possible to do so in local settings due to many pragmatic constraints. As an alternative approach to gain physical insight into three distinctive nanosystems considered in this thesis, the detailed dynamics of thermally-induced effects at atomistic level are computationally ‘measured’ through MD instead. The following problems are the core concerns to be addressed in this thesis:

1. What is the dynamical mechanism that drives the formation of graphene islands on the (0001) surface of a 6H-SiC substrate?
2. When heated up from room temperature, at what temperature graphene begins to form on the (0001) surface of a 6H-SiC substrate?
3. How to use MD to simulate the epitaxial growth of multilayered graphene on the (0001) surface of a 6H-SiC substrate?
4. When heated up from room temperature, at what temperature a free-standing graphene begins melt?
5. What happens to the surface atoms of a nano size ZnO slab upon heating beyond 1000 K?
6. When heated up from room temperature, will oxygen be released from the surfaces of a ZnO slab of nano size? If they do, will they be released in the form of monoatom or molecular? At which temperature oxygen begins to sublimate?

1.3 Objectives

The aim of the research presented is to perform MD simulation on epitaxial growth of graphene on 6H-SiC (0001) substrate [2]. A prediction regarding the temperature of the formation of graphene on 6H-SiC (0001) substrate is being made. The quality (numbers of hexagonal rings formed) of graphene is determined. The aim of this project is to come up with an effective strategy and method such as binding energy, average bond length and pair correlation function to qualitatively and quantitatively to determine the formation of graphene. The objective is to come up with the optimal condition of annealing of high quality graphene.

Next, the melting point of silicene is determined through MD simulations. MD simulations is used to quantify the melting points of graphene through some physical quantities such as caloric curve, pair correlation function and global similarity index. A novel indicator known as global similarity index was used to predict the melting point of the silicene and compare it with the existing conventional methods.

Finally, the surfaces of oxygen-terminated and zinc-terminated ZnO slab is characterized using MD simulations via annealing. The results thus obtained are compared with those experimental results obtained in Sharom et al. [3]. experiment (which will be detailed in Chapter 3 and Chapter 4). The vacancies formed at the surfaces of annealed ZnO slab is evaluated for various temperatures and charges distribution is quantified.

All the simulations above will be compared with the existing experimental results and to predict the thermal behavior of the above selected nanostructures, the reliability of MD simulations is then determined.

1.4 Overview of the thesis

An introduction to the research presented in the theses, motivations, problem statements and objectives were provided in Chapter 1 of the thesis. Chapter 2 is generally a literature review and background theory of some selected nanostructures such as carbon nanostructures (graphene especially will be made as the priority subject), history of the epitaxial growth of graphene, silicene and some background of zinc oxide. Chapter 3 will focus on methodology such as the implementation of empirical potential, construction of the nanostructures and simulation details. Chapter 4 presents the findings and results of the MD simulations on all three nano systems, namely, 6H-SiC (0001), free-standing silicene and ZnO nano slab. Chapter 5 will be the conclusion of this thesis.

CHAPTER 2: BACKGROUND THEORY

2.1 Carbon Nanostructures

Carbon nanostructures comprising fullerene (0-D), carbon nanotubes (1-D), graphene (2-D) and graphite (3-D) are all but derived from carbon and has a characteristic dimension of a few or tens of nanometer in size. Most of these carbon nanostructures are sp^2 -hybridized. The bond length between carbon chains is approximately 1.42 Å. Carbon nanostructures as shown in Fig. 2.1 have attracted researchers around the world due to their superior and unique proprieties as compared to their bulk materials, especially in optical, semiconducting and mechanical properties [4]. However, these nanostructures are rarely produced as free-standing entities but are often grown on a substrate by using a suitable catalyst. The first graphene sheet was synthesized through “scotch tape cleaving” method of on three-dimensional graphite. The synthesis is halted when it reaches a single layer of carbon atoms [5].

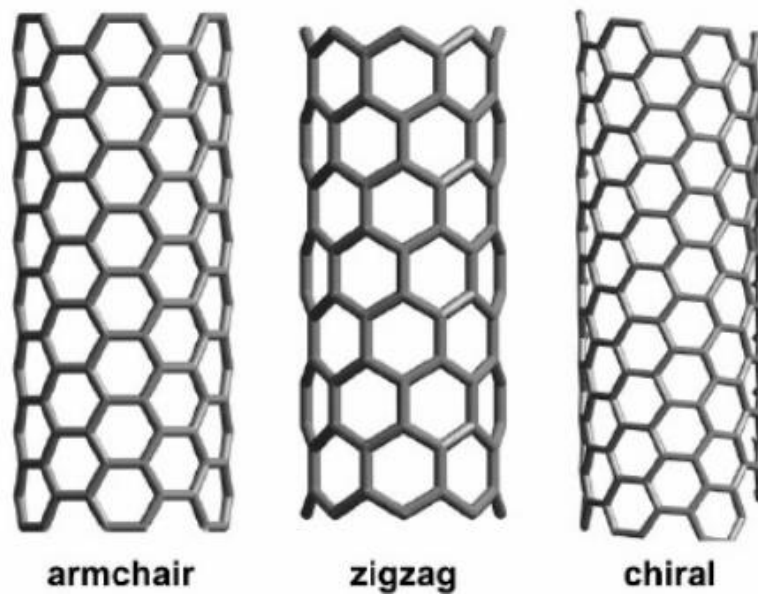


Figure 2.1: Types of carbon nanotubes and its chirality.

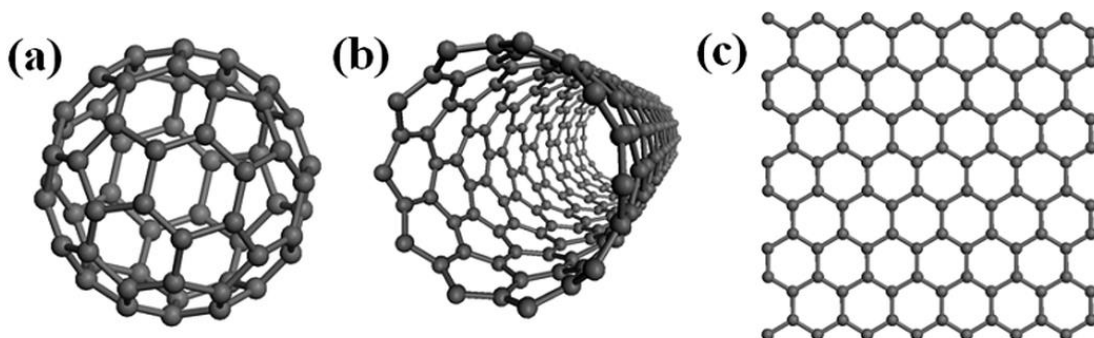


Figure 2.2: Low-dimensional carbon allotropes: (a) fullerene (0-D), (b) carbon nanotube (1-D) and (c) graphene (2-D).

To fully understand the nature of graphene, the attention is first turn to carbon nanotubes. If one cuts along the wall parallel to the axis running through the cylinder, and roll out, a two-dimensional graphene is formed. Fig. 2.1 shows carbon nanotubes with three different chirality, namely armchair, zig-zag and chiral. The chirality of the nanotubes hinges on the orientation of the tube and the rolling angle. The tube chirality of chiral vector defines the characteristics of a carbon nanotube. The chiral vector, \mathbf{C} , \mathbf{a}_1 and \mathbf{a}_2 are as shown in Fig. 2.3. Mathematically, these three parameters can be written as the combination of lattice basis vector,

$$\mathbf{C} = n\mathbf{a}_1 + m\mathbf{a}_2 \quad (2.1)$$

The integers (n, m) denote the number of steps along the zig-zag carbon bonds of the hexagonal lattice while \mathbf{a}_1 and \mathbf{a}_2 are the unit vectors. Zig-zag and armchair configurations of carbon nanotubes can only be observed under limited circumstances when the chiral angle, θ , is at 0° and 30° respectively due to the geometry of the carbon bonds around the circumference of the nanotube.

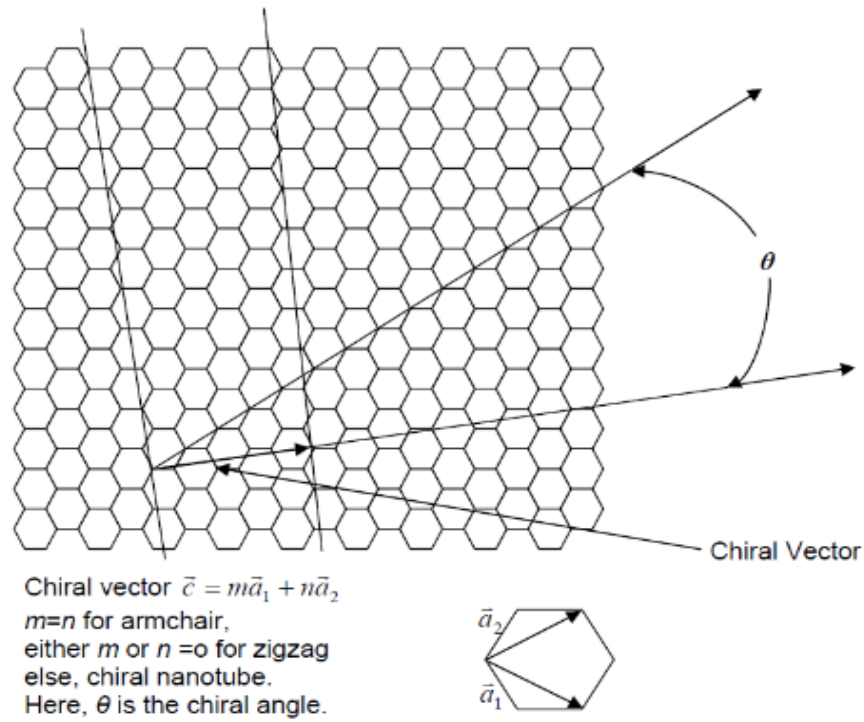


Figure 2.3: The nanotubes and its chiral angle.

The length of chiral vector is defined as the circumference of the carbon nanotube. The diameter, d , of the nanotube is thus

$$d = \frac{c}{\pi}$$

$$= a\sqrt{n^2 + mn + m^2} \quad (2.2)$$

Lattice constant a of 2.49 Angstrom of the carbon honeycomb is also the lattice parameter for carbon nanotube.

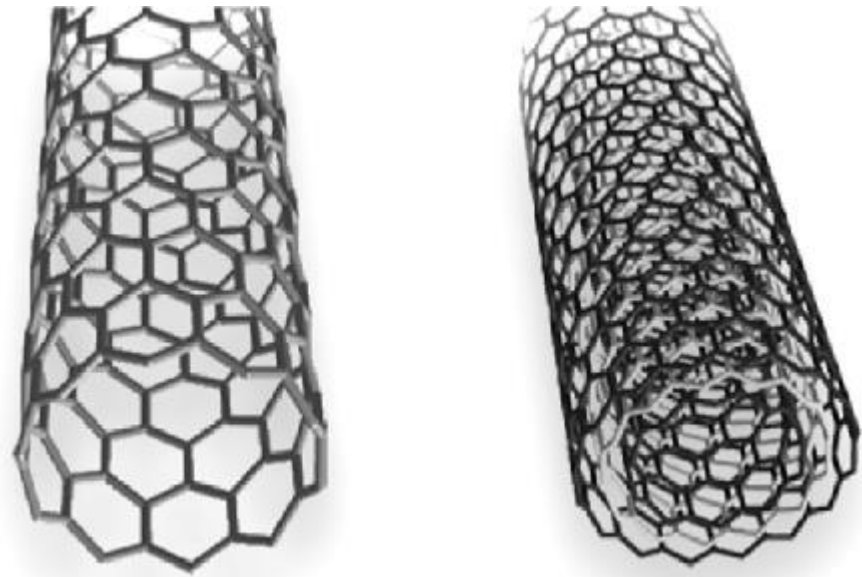


Figure 2.4: Single wall nanotube (left) and multiwall nanotube (right).

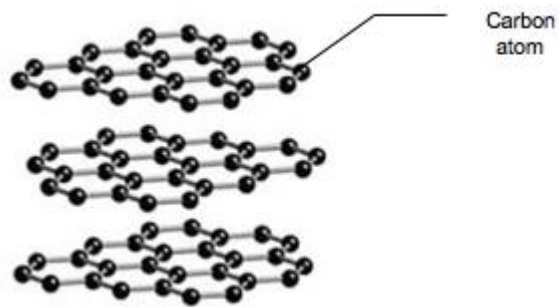


Figure 2.5: A graphite structure.

The carbon nanostructures are generally greyish-black in color, opaque and have a lustrous black sheen. Both metal and non-metal properties can be observed in the carbon nanostructures. It is hard but brittle. It has excellent thermal and electrical conductivity and is chemically inert. The stacking of graphene sheets will form graphite as shown in Fig. 2.5. The interlayer spacing between the carbon layers is 3.35 Å. A three-million-layer graphene will form bulk graphite with an aggregate layer thickness of 1 mm [6].

2.2 Epitaxial growth of graphene

The discovery of graphene has revolutionized our fundamental understanding of material science. This unique two-dimensional nanostructure comprising pure monolayer carbon atoms formed sp , sp^2 and sp^3 hybridization, allowing more stable formation as compare to other carbon allotrope. Notable electronic properties are high electrical conductivity (typically $\sim 2 \text{ m}\Omega^{-1}$) [7] or high carrier mobility [8] (typically $\sim (2 - 5) \times 10^3 \text{ cm}^2 \text{ V}^{-1}$) (value as high as $5 \times 10^3 \text{ cm}^2 \text{ V}^{-1}$ has been reported also [9]) and superior thermal conductivity ($\sim 3 - 5 \times 10^3 \text{ Wm}^{-1} \text{ K}^{-1}$) [10]. Single-layer graphene also presents unusual mechanical properties such as high-in-plane stiffness (single-layer graphene with an effective thickness $\sim 6 \text{ \AA}$) and extremely hard [11], i.e. intrinsic strength around 130 Gpa or Young's modulus value around 1 Tpa).

A number of studies have been conducted for pre-graphene formation on the SiC surface by using scanning tunneling and atomic force microscopy, providing detailed view on the surface reconstruction of SiC surface [12]. Experimentally, several methods reported producing high quality graphene layers. One popular

method is the epitaxial graphene technique, where 4H- or 6H-SiC surfaces are heated up to high temperature. Epitaxial growth refers to the deposition of a crystalline overlayer on a crystalline substrate. This strategy involves graphitization of SiC whereby Si sublimation occurred during high temperature annealing in vacuum. To gain insight into the growth of epitaxial graphene, Hannon and Tromp [13] studied the formation of graphene using the low-energy electron microscopy. It is worth noting that Hannon and Tromp observed the formation of smooth steps and the step height was measured through atomic-force microscopy under prolonged high temperature annealing at 1298 K in vacuum. It is believed that this terracing feature would give rise to pit formation which hinders the formation of flat graphene layers at temperature $T < 1300$ K. In a separate study, Borysiuk et al. [14] independently observed similar carpet-like corrugation panorama using transmission electron microscopy. Recent works of Tang *et al.* [15], Lampin *et al.* [16], Jakse *et al.* [17] using computer simulation have also provided important insights on the formation of epitaxial graphene.

The occurrence of epitaxial graphene is not only limited to SiC substrate but is also extended to various transition elements. Li *et al.* successfully grew large area of graphene on Cu (1 1 1) surface [18] and Sutter et al. surprisingly fabricated a large graphene domain with uniform thickness across Ru metal surface [19]. Computer simulation has also been conducted by Enstone *et al.* by using Monte Carlo model on graphene/Cu (1 1 1) [20]. To differentiate graphene from the substrate, it is to be noted that the graphene that grew epitaxially has the advantage of having higher electronic carrier mobility relative to the SiC substrate. It is, however, important to note also that removal of graphene from its respective metal substrate might damage the graphene layer.

2.3 Silicene

Silicene, a two-dimensional nanosheet made up of silicon atoms arranged in the form of honey comb lattice, has been predicted theoretically by Takeda and Shiraishi [21] in year 1994. Subsequent DFT calculations by Guzman-Verri and Voon [22] revived the interest on silicene by showing that silicene was indeed energetically stable, and of feasible possibility to being experimentally produced. Silicene, unlike graphene which prefers sp^2 hybridization, is not flat. Rather, due to the preference of sp^3 hybridization, the silicene sheet has a buckled configuration, where the out-of-plane buckle parameter is predicted to be 0.44 \AA according to DFT calculations. Having a close resemblance to graphene, silicene offers many possibilities as a functional material of advanced applications, such as photovoltaic, optoelectronic devices [23], thin-film solar cell absorbers beyond bulk Si [24] and hydrogen storage [25]. One advantage of silicene over other 2D materials is that it is, in principle, easier to get integrated into nano devices which are mainly silicon-based.

Silicene is a rather new form of 2D material and was synthesized on supported substrates in a series of discovery since 2007 [26]. Following the successful synthesis of silicene on supported substrate, many theoretical studies and simulations on the structural, mechanical, electronic and thermal properties of silicene on supported substrate have been published [27]. The structural properties of a free-standing silicene sheet, as was originally investigated by Jose *et al.* [25], however, being modified when grown on a substrate. Thus, the silicene experimentally synthesized so far is not free-standing but sitting on a substrate. One has yet to see any report of experimentally synthesized free-standing silicene. Having

said that, investigation of free-standing silicene serves the purpose of understanding the pristine system in the absence of interactions with surfaces. The understanding on the basic properties of silicene without the interference from substrate shall provide useful insight for higher level manipulation of silicene. One of the envision is the ‘van der Waals’ heterostructures envisaged by Geim [27], which it deals with heterostructures and devices made by stacking different 2D crystals on top of each other. Strong covalent bonds provide in-plane stability of 2D crystals, whereas relatively weak, van der Waals-like forces are sufficient to keep the stack together.

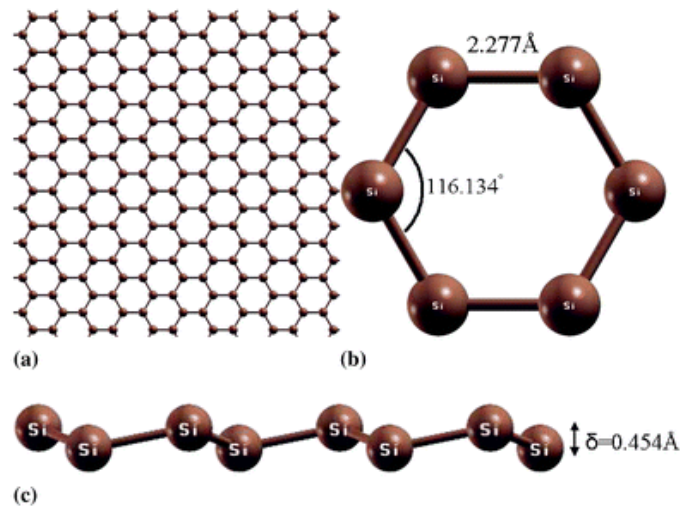


Figure 2.6: (a) The structure of a free-standing silicene, (b) the bond length and bond angle of silicene and (c) the buckling parameter of a silicene.

In this thesis, there are very limited work on the melting behavior and thermal stability of free-standing silicene is reported in the literature. Bocchetti *et al.* simulated the melting behavior of free-standing silicene via Monte Carlo method with original and modified version of Tersoff potential parameter set (known as ARK) for silicon atom [28]. According to Bocchetti *et al.*, original Tersoff parameters for silicon atom results in a melting of the free-standing silicene at 3600 K, meanwhile the melting temperature obtained using ARK parameter set is only ~

1750 K. Berdiyrov et al. simulated the influence of defect on the thermal stability of free-standing silicene via MD using Reactive force-field (ReaxFF) [29], where it is found that pristine silicene is stable up to 1500 K. As a general observation, melting properties and thermal stability of free-standing silicene obtained in MD simulations varies from cases to cases depending on the details of the simulation procedure. Furthermore, the simulation results are strongly force-field dependent. Apart from simulating thermal stability, MD simulation has also been applied to investigate or predict thermal conductivity of free-standing silicene. A wide range of potentials is employed in these simulations, and the potentials are of semi-empirical type. For example, Zhang *et al.* developed a set of Stillinger-Weber potential parameters specifically for a single-layer Si sheet to simulate the thermal conductivity [30]. Most researchers would often use Tersoff potential with original parameter sets though.

2.4 Zinc Oxide

Zinc oxide (ZnO) has been extensively studied, both theoretically and experimentally, due to its many promising applications in piezoelectric devices, transistors, photodiodes, photocatalysis and antibacterial function [31-33]. The physical properties of ZnO, especially its surface properties, can be experimentally modified at the atomic level to engineer the material for desired functionality. Since ZnO contacts with its external environment through its surfaces, knowing how the surface properties respond to external perturbation (e.g. thermal treatment) would provide valuable information on how to manipulate ZnO for application purposes in future. And one of the simplest way researchers known is to heat ZnO to high

temperature (below its melting point). Heating ZnO can be easily carried out in practice, and many works had been reported along this line [34-36].

ZnO crystals are dominated by four surfaces with low Miller indices: the non-polar $(1\ 0\ \bar{1}\ 0)$ and $(1\ 1\ \bar{2}\ 0)$ surfaces and the polar surfaces which are the zinc-terminated surface $(0\ 0\ 0\ 1)$ and the oxygen terminated surface $(0\ 0\ 0\ \bar{1})$. Surface energy of polar surfaces in an ionic model diverges with sample size due to the generation of macroscopic electrostatic field across the crystal [37]. This kind of behavior was well investigated by Tasker [38]. Accordingly, wurzite ZnO is also labeled as Tasker-type surfaces, and these surfaces are formed by alternating layers of oppositely charged ions.

It is interesting to investigate what will happen to the atomic configuration of the surface when a ZnO slab with finite thickness is heated without melting. Sublimation of atoms from the polar surfaces due to temperature effect will be studied using molecular dynamics (MD) simulation, where the trajectories of all atoms at a given temperature T are followed quantitatively. As will be reported in Chapter 4 when the result of the MD simulation of ZnO is represented, in which the reactive force field (ReaxFF) for ZnO is used, sublimation of O atoms from ZnO polar surface is observed. ReaxFF for ZnO allows bond formation and charge transfer among the selected atoms. When sublimation of atoms occurs, point vacancies are created on the surface. Quantitative information of the amount and type of atoms sublimated, as well as point vacancies created on the surface at different annealing temperatures can thus be obtained.

Experimentally, if a ZnO wurzite surface is heated to an elevated temperature and investigate the resultant surface using photoluminescence (PL)

measurement, the spectrum should reflect the amount of point vacancies created. It is expected that an increase of annealing temperature will create more point vacancies. In this thesis, predictions from MD simulation are compared with PL data.

2.5 Molecular Dynamics Simulation

Molecular dynamics (MD) simulation is used to solve equation of motion of particles in different phases [39]. It could reliably predict the physical properties of material even in non-ground state. Particles interact with each other at finite temperature for an extended period in a MD simulation. The atoms or molecules evolve in the system made possible by the interactive forces or so-called empirical inter-atomic potential. The forces that govern the motion of atom are in accordance with Newton's Second law. Using equation of motions of all particles in the system, the evolution of the system is solved as,

$$\frac{dr_i}{dt} = v_i \quad (2.3)$$

$$\frac{d}{dt}(m_i v_i) = F_i = -\nabla_i V = -\nabla_i [\Sigma_j V_2(r_i, r_j) + \Sigma_{j,k} V_3(r_i, r_j, r_k) + \dots] \quad (2.4)$$

where i denotes the particle in the system, V is the interactive potential between particles, r_i is the position of the particles while v_i refers to the velocity of the system.

The initial conditions to commence an MD simulation include positional coordinates, initial random seed of the velocity and appropriate empirical potential (which will be elaborated in detail in Chapter 3) so as to derive the forces between particles. Regardless of the merits of the other algorithms in the simulation code (integrators, pressure and thermostat etc.), whether or not the simulation produces

realistic results depends ultimately on the empirical potential. Empirical potentials are also the computationally most intensive parts of a molecular dynamics simulation code, consuming up to 95% of the total simulation time. The simulated particles are placed in the simulation box with a defined boundary condition. There are two types of boundary condition: periodic boundary condition and fixed boundary condition. Periodic boundary condition eliminates the edge effect on the simulation box. Periodic boundary condition artificially creates the simulation box with infinite volume appropriate for simulating bulk or periodic crystal. This is achieved by replicating the simulation box in such a way that the particles within the simulation box would interact with their neighboring particles. As for fixed boundary condition, the simulation box is enclosed by “wall” or “edge” with a defined volume. The particles would be reflected to the simulation box when the interacting particles reach the boundary of the simulation box. This fixed boundary is suitable for the simulation of finite size particles such as clusters, surfaces and nanoparticles.

It is essential that thermalization process is performed onto the system to enable the system to achieve thermal equilibrium and minimum energy. Microcanonical ensemble (NVT) with Nose-Hoover [40] thermostat is best used to equilibrate a system to its local minima. The molarity, volume and temperature of the system are conserved. The ensemble performs time integration on Nose-Hoover style non-Hamiltonian equations of motion to generate positions and velocities. When used correctly, the time-averaged temperature of the particles will match the target values specified [41]. Sometimes, canonical ensemble (NVE) is also used, during which the system molarity, volume and energy are conserved. Thus, the equilibrating of the system can also be ascertained using NVE. The summary of concept of periodic boundary condition is shown in Figure 2.7.

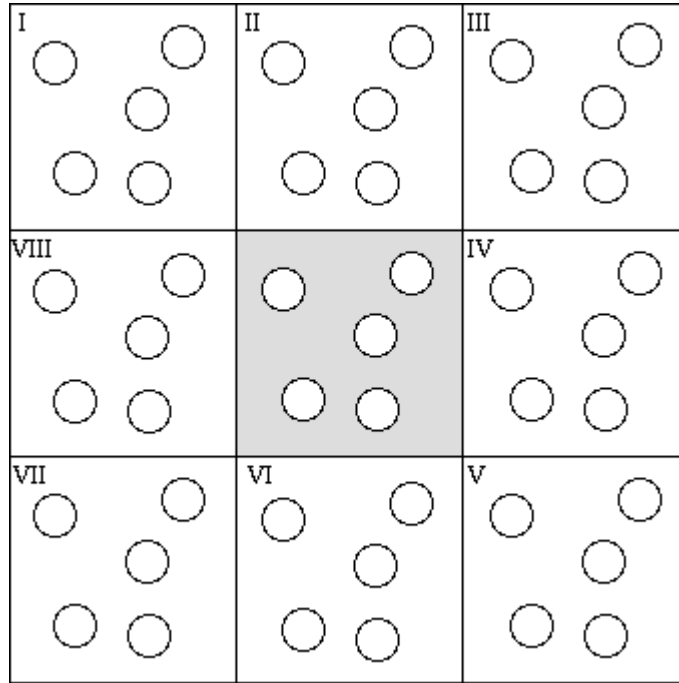


Figure 2.7: Periodic boundary condition of molecular dynamics. Each particle not only interacts with every other particle in the system but also with all other particles in the copies of the system.

In practice, MD simulation is performed by using existing computational packages. There exist many full-fledged, multi-functional software packages implementing MD. The code Large-scale Atomic/Molecular Massively Parallel Simulator (LAMMPS) [42] is among the best known. It will be used exclusively in this thesis for simulating the thermal behavior of the three chosen nanosystems.

CHAPTER 3: RESEARCH METHODOLOGY

3.1 Epitaxial Growth of Graphene

3.1.1 Empirical Potential

Simulation of epitaxial graphene growth involve Si and C atoms. In the context of MD simulation, the so-called force field, which refers to the interaction among these atoms has to be determined. The force field used in a MD simulation plays a vital role as the correctness of the simulated results is directly determined by it. For the case of carbon and silicon atoms, due to their wide applications in current materials science and semiconducting technology, many high-quality force fields have been historically developed. Considered as the most widely used in MD simulation of materials science involving carbon and silicon atoms is the prototype force field by Tersoff [43] and its more refined form, or the so-called TEA potential (Tersoff-Erhart-Albe) [44]. Both are empirical force fields developed based on experimental input and rigorous physical consideration. These two force fields will be used in simulating the epitaxial growth of graphene on the SiC substrate.

Tersoff or TEA force field has the following general expression,

$$E = \sum_i E_i = \frac{1}{2} \sum_{j \neq i} V(r_{ij}) \quad (3.1)$$

where E_i denotes the total energy for an atom at site i . The location of the site is denoted r_i . The potential energy, $V(r_{ij})$, arising from the interaction between an atom at site r_i and another at site r_j , where both are separated by a distance r_{ij} , is assumed to take the following form in the original Tersoff paper,

$$V(r_{ij}) = f_c(r_{ij})[a_{ij}V_R(r_{ij}) + b_{ij}V_A(r_{ij})] \quad (3.2)$$

in which f_c is a cutoff function varying continuously from 1 to 0 around the position $(S_{ij} + R_{ij})/2$, where they are defined as per $S_{ij} = (S_i S_j)^{1/2}$ and $R_{ij} = (R_i R_j)^{1/2}$. S_{ij} and R_{ij} respectively define the cutoff distance around $(S_{ij} - R_{ij})/2$ for atoms located at the first-neighbor shell. Based on the ideas suggested in Tersoff's original papers [49, 50], the function f_c is chosen to take the form

$$f_c(r_{ij}) = \begin{cases} 1, \\ \frac{1}{2} + \frac{1}{2} \cos[\pi(r_{ij} - R_{ij})/(S_{ij} - R_{ij})], & R_{ij} < r_{ij} < S_{ij}, \\ 0, \end{cases} \quad (3.3)$$

where i and j stands for C or Si. The first term in Eq. (3.2) (denoted by the subscript "R") represents a repulsive part, whereas the second (denoted by the subscript "A") an attractive one. $V_R(r_{ij})$ and $V_A(r_{ij})$ in the square brackets in Eq. (3.2) are both expressed in the Morse potential form, namely,

$$\begin{aligned} V_R(r_{ij}) &= A_{ij} \exp[-\lambda_{ij}(r_{ij} - r_{ij}^{(0)})] \\ V_A(r_{ij}) &= -B_{ij} \exp[-\mu_{ij}(r_{ij} - r_{ij}^{(0)})]. \end{aligned} \quad (3.4)$$

The coefficients in Eq. (3.4) are defined via $A_{ij} = (A_i A_j)^{1/2}$, $B_{ij} = (B_i B_j)^{1/2}$, whereas coefficients in the exponents are $\lambda_{ij} = (\lambda_i + \lambda_j)/2$ and $\mu_{ij} = (\mu_i + \mu_j)/2$.

It is reasonable to assume that the interaction among the atoms is effective up to a distance set by the first-neighbor shell. Such assumption leads an approximated expression for the coefficient a_{ij} , namely, $a_{ij} = 1$.

b_{ij} is much complicated quantity. It measures the bond order describing the coordination of atoms i and j . Cast in the most general form, it reads

$$b_{ij} = \chi_{ij} (1 + \beta_i^{n_i} \zeta_{ij}^{n_i})^{-\frac{1}{2n_i}}, \quad (3.5)$$

where the parameter χ_{ij} plays the role of strengthening or weakening the heteropolar bonds, relative to the value estimated by interpolation, and

$$\zeta_{ij} = \sum_{k \neq i, j} f_c(r_{ik}) g(\theta_{ijk}) \exp[v_{ij}^m (r_{ij} - r_{ik})^m]. \quad (3.6)$$

Eq. (3.7) contains the three-body interaction function

$$g(\theta_{ijk}) = \gamma_{ik} \left[1 + \frac{c_{ik}^2}{d_{ik}^2} - \frac{c_{ik}^2}{d_{ik}^2 + (h_{ik} - \cos \theta_{ijk})^2} \right] \quad (3.7)$$

In Eq. (3.7), θ_{ijk} is the bond angle between bond ij and any atom at k ($\neq i, j$) bonded with atom i forming bond ik , and constants γ_{ik} , c_{ik} , d_{ik} and h_{ik} are accordingly determined by three-body interactions.

3.1.2 Construction of 6H-SiC substrate

To begin with the MD simulation, a data file containing the details of the positions of all atoms in the unit cell and the lattice parameters of a 6H-SiC (0001) crystal has to be first prepared. The information of the crystal structure of the 6H-SiC (0001) substrate was obtained from the NRL (Naval Research Laboratory) structure database [45], and is reproduced in Table 3.1.

```

Primitive vectors
a(1) = 1.54035000 -2.66796446 .00000000
a(2) = 1.54035000 2.66796446 .00000000
a(3) = .00000000 .00000000 15.11740000

```

Volume = 124.25290558

```

Reciprocal vectors
b(1) = .32460155 -.18740879 .00000000
b(2) = .32460155 .18740879 -.00000000
b(3) = -.00000000 .00000000 .06614894

```

Basis Vectors:						
Atom	Lattice Coordinates		Cartesian Coordinates			
C	.00000000	.00000000	.12540000	.00000000	.00000000	1.89572196
C	.00000000	.00000000	.62540000	.00000000	.00000000	9.45442196
W	.00000000	.00000000	.00000000	.00000000	.00000000	.00000000
W	.00000000	.00000000	.50000000	.00000000	.00000000	7.55870000
C	.33333333	.66666667	.79190000	1.54035000	.88932149	11.97146906
C	.66666667	.33333333	.29190000	1.54035000	-.88932149	4.41276906
C	.33333333	.66666667	.45840000	1.54035000	.88932149	6.92981616
C	.66666667	.33333333	-.04160000	1.54035000	-.88932149	-.62888384
W	.33333333	.66666667	.66670000	1.54035000	.88932149	10.07877058
W	.66666667	.33333333	.16670000	1.54035000	-.88932149	2.52007058
W	.33333333	.66666667	.33320000	1.54035000	.88932149	5.03711768
W	.66666667	.33333333	-.16680000	1.54035000	-.88932149	-2.52158232

Table 3.1: LAMMPS input requires for the data files which provides information required for constructing a rhombus shape 6H-SiC substrate. The information was extracted from <http://cst-www.nrl.navy.mil/lattice/struk/6h.html> [45].

The numerical values of the primitive vectors $\mathbf{A}_1, \mathbf{A}_2, \mathbf{A}_3$ (correspond to $a(1), a(2), a(3)$ in Table 3.1) are, according to the NRL database,

$$\mathbf{A}_1 = \{1.54035000, -2.66796446, 0.00000000\},$$

$$\mathbf{A}_2 = \{1.54035000, 2.66796446, 0.00000000\},$$

$$\mathbf{A}_3 = \{0.00000000, 0.00000000, 15.11740000\},$$

in nanometers. In a more conventional notation, the three primitive vectors $\mathbf{A}_1, \mathbf{A}_2, \mathbf{A}_3$ are denoted $\mathbf{a} \equiv \mathbf{A}_1, \mathbf{b} \equiv \mathbf{A}_2, \mathbf{c} \equiv \mathbf{A}_3$ respectively. The norm of $\mathbf{a}, \mathbf{b}, \mathbf{c}$, denoted by a, b, c , are the three lattice constants defining the SiC unit cell. The value of a can be easily solved for, as per

$$\mathbf{a}^2 = \mathbf{A}_1^2 = 1.54035000^2 + 2.66796446^2 = \left(\frac{a}{2} \mathbf{X} - \frac{\sqrt{3}a}{2} \mathbf{Y} \right)^2 = a^2$$

$$\Rightarrow a = 3.08$$

$$\mathbf{b}^2 = \mathbf{A}_2^2 = 1.54035000^2 + 2.66796446^2 = \left(\frac{a}{2} \mathbf{X} - \frac{\sqrt{3}a}{2} \mathbf{Y} \right)^2 = b^2$$

$$\Rightarrow b = a = 3.08.$$

$\mathbf{X}, \mathbf{Y}, \mathbf{Z}$ denote the elemental basis vectors, namely, $\mathbf{X} = \{1,0,0\}, \mathbf{Y} = \{0,1,0\}, \mathbf{Z} = \{0,0,1\}$. Since 6H-SiC belongs to the hexagonal class, by definition, $b = a, \alpha = \beta = 90^\circ$ and $\gamma = 120^\circ$, where α is the angle between the lattice vectors \mathbf{a} and \mathbf{c} , β the angle between the lattice vectors \mathbf{b} and \mathbf{c} , γ the angle between the lattice vectors \mathbf{a} and \mathbf{b} . The lattice parameter c is simply the norm of $\mathbf{A}_3, c = 15.12$, The unit cell for the SiC crystal so constructed is rhombus in shape. However, LAMMPS does not support direct input for the angles of hexagonal lattice. The lattice constants a, b, c and angles in the form of α, β and γ need to be converted into LAMMPS-readable form, lx, ly, lz, xy, xz and yz . The conversion is shown in Equation 3.8.

$$\begin{aligned}
lx &= a \\
xy &= b \cos \gamma \\
xz &= c \cos \beta \\
ly^2 &= b^2 - xy^2 \\
yz &= \frac{b * c \cos \alpha - xy * xz}{ly} \\
lz^2 &= c^2 - xz^2 - yz^2
\end{aligned}
\tag{3.8}$$

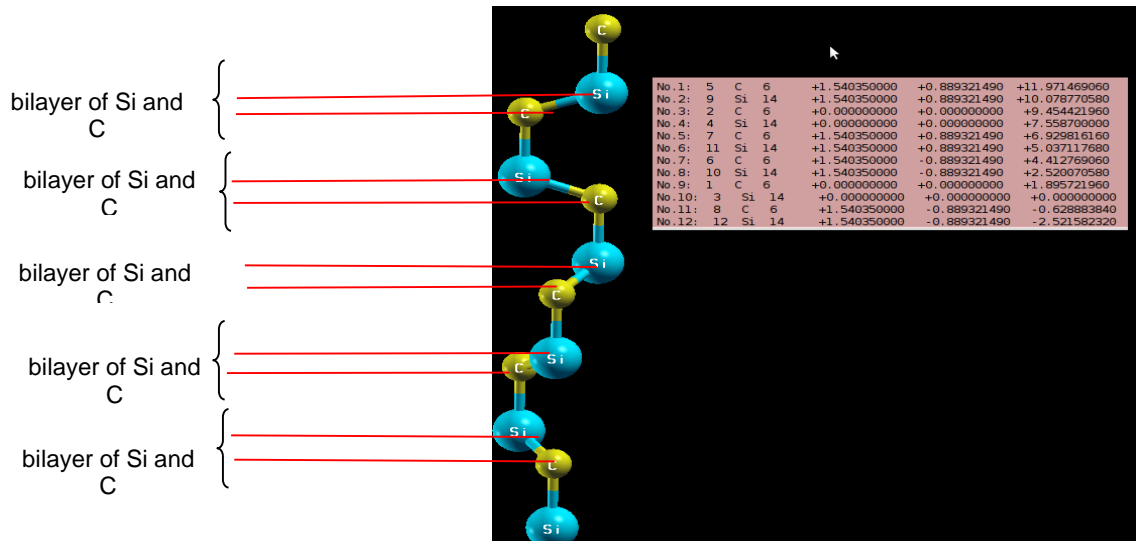


Figure 3.1: Visualization of the SiC unit cell. Si atom is in light blue. The type of atom can be read off from column 3 in the inset. The z-coordinate of each atom, which are labeled No. 1 to No. 12 in the first column of the inset, are clearly shown in the last column of the inset.

There is a total of 12 atoms in a unit cell of a 6H-SiC crystal, see Figure 3.1. Coordinates of each atom in the unit cell are also displayed. The last column in the figures of Fig. 3.1 refers to the z-coordinates of the respective atoms. Vertical distance between the atoms can be deduced from their z-coordinates straightforwardly. The unit cell when repeated along the x-direction and y-direction via periodic boundary condition will form an infinite substrate along these two